Hydrothermal Syntheses of Metal–Organic Frameworks Constructed from Aromatic Polycarboxylate and 4,4′-Bis(1,2,4-triazol-1-ylmethyl)biphenyl

ARTICLE *in* CRYSTAL GROWTH & DESIGN · MAY 2011

Impact Factor: 4.89 · DOI: 10.1021/cg101494t

6 AUTHORS, INCLUDING:

Junhong Fu
Australian National University
9 PUBLICATIONS **80** CITATIONS

SEE PROFILE

CRYSTAL GROWTH & DESIGN

ARTICLE

pubs.acs.org/crystal

Hydrothermal Syntheses of Metal−Organic Frameworks Constructed from Aromatic Polycarboxylate and 4,4′-Bis(1,2,4-triazol-1-ylmethyl)biphenyl

Yajuan Mu, Junhong Fu, Yajing Song, Zhen Li, Hongwei Hou,* and Yaoting Fan

Department of Chemistry, Zhengzhou University, Zhengzhou, Henan 450052, P. R. China

Supporting Information

ABSTRACT: Six new metal−organic frameworks, namely, $\{[Co(btmb)(HBTC)]\cdot 2H_2O\}_n$ (**1**), $\{[Co_3(btmb)_3(BTC)_2(H_2O)_2]\cdot 6H_2O\}_n$ (**2**), $\{[Co_3(btmb)_3(BTC)_2(H_2O)_4]\cdot 2H_2O\}_n$ (**3**), $\{[Ni_3(btmb)_3(BTC)_2(H_2O)_4]\cdot 2H_2O\}_n$ (**4**), $[Cu(btmb)(HBTC)]_n$ (**5**), and $[Cu(btmb)(NDC)]_n$ (**6**) (H_3BTC = 1,3,5-benzenetricarboxylic acid, H_2NDC = 1,2-benzenedicarboxylic acid, and btmb = 4,4′-bis(1,2,4-triazol-1-ylmethyl)biphenyl), have been synthesized under hydrothermal conditions. The structure of **1** is a 6-connected self-penetrating three-dimensional (3D) framework with $4^4\cdot 6^{10}\cdot 8$ topology. Complex **2** exhibits a trinodal (3,4)-connected topology with a Schläfli symbol of $(6^2\cdot 8^4)(6^4\cdot 8^2)(6^3)$. Both complexes **3** and **4** possess 3D pillar-layered structures with a Schläfli symbol of $(6^2\cdot 8\cdot 10^3)(6^4\cdot 8\cdot 10)(6\cdot 10^2)$. Complex **5** is also a 3D polymer with a pillar-layered framework, which can be simplified as the $(6^3)(6^9\cdot 8)$ topology. Complex **6** shows a 4-connected 3D framework with a Schläfli notation of $(6^5\cdot 8)_2$. Furthermore, complexes **1**−**6** as heterogeneous catalysts were studied in the green catalysis process of the oxidative coupling of 2,6-dimethylphenol (DMP) to poly(1,4-phenylene ether) (PPE) and diphenoquinone (DPQ). The results show that these complexes exhibit different catalytic activities; both the Cu complexes are catalytically active by showing high conversion of DMP and high selectivity of PPE, and they exhibit great potential as recyclable catalysts.

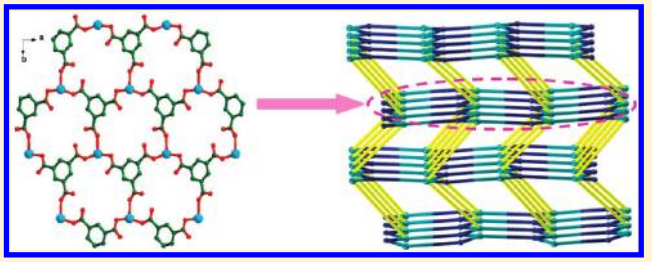

INTRODUCTION

The rational design and construction of novel metal−organic frameworks (MOFs) continues to be a productive research area, owing to their fascinating structural diversities and potential application as new materials.[1] Of the many rational approaches to the design of these materials, the route of selecting well-designed organic ligands as building blocks with metal ions or metal clusters as nodes has been proven to be an efficient strategy. However, predicting and accurately controlling the framework array of a given crystalline product still remains a considerable challenge, due to the fact that the subtle self-assembly process is frequently influenced by numerous other factors, such as the presence of auxiliary ligands or solvent, concentration, counteranion, temperature, the pH value of the solution, and so on.[2] Therefore, further studies are required to understand the roles of these factors in the formation of MOFs.

In the design and syntheses of MOFs, aromatic multicarboxylate ligands, especially, benzenedicarboxylate and benzenetricarboxylate, are excellent building blocks, not only because of their various coordination modes to metal ions, resulting from completely or partially deprotonated sites allowing for the large diversity of topologies, but also because of the strong coordinating ability of carboxylates, which can lead to good thermal stabilities of the materials and increase the possibility of their functionalization.[3] Meanwhile, the results of previous studies show that flexible bis(triazole) ligands can adopt a variety of conformations according to the restrictions imposed by the coordination geometry of the metal ions.[4] So, the flexible bis(triazole) ligands can also serve as one kind of most useful organic linker for constructing MOFs with versatile topologies.

Recent investigations have demonstrated that the employment of mixed organic ligands, especially the mixed polycarboxylate and N-containing ones, during the self-assembly process, has been widely adopted for the construction of MOFs with novel structures and unique properties.[5] Following such a mixed ligand strategy, to further understand the coordination chemistry of the flexible bis(triazole) spacer and rigid aromatic polycarboxylate acids, and to explore new materials with beautiful architectures and good physical properties, in this work, we selected the long flexible bis(triazole) ligand btmb as organic linker in the presence of H_3BTC and H_2NDC as coligands, and we hydrothermally synthesized six new MOFs with intriguing structures, $\{[Co(btmb)(HBTC)]\cdot 2H_2O\}_n$ (**1**), $\{[Co_3(btmb)_3(BTC)_2(H_2O)_2]\cdot 6H_2O\}_n$ (**2**), $\{[Co_3(btmb)_3(BTC)_2(H_2O)_4]\cdot 2H_2O\}_n$ (**3**), $\{[Ni_3(btmb)_3(BTC)_2(H_2O)_4]\cdot 2H_2O\}_n$ (**4**), $[Cu(btmb)(HBTC)]_n$ (**5**), and $[Cu(btmb)(NDC)]_n$ (**6**), where

Received: November 10, 2010
Revised: April 15, 2011
Published: April 20, 2011

Table 1. Crystallographic Data and Structure Refinement Details for 1−6

compound	1	2	3	4	5	6
formula	$C_{27}H_{24}CoN_6O_8$	$C_{72}H_{66}Co_3N_{18}O_{20}$	$C_{72}H_{66}Co_3N_{18}O_{18}$	$C_{72}H_{66}Ni_3N_{18}O_{18}$	$C_{27}H_{20}CuN_6O_6$	$C_{26}H_{20}CuN_6O_4$
fw	619.45	840.11	1648.22	1647.56	588.03	544.02
T/K	293(2)	293(2)	293(2)	293(2)	293(2)	293(2)
λ (Mo Kα), Å	0.71073	0.71073	0.71073	0.71073	0.71073	0.71073
cryst syst	monoclinic	monoclinic	monoclinic	monoclinic	monoclinic	triclinic
space group	$P2_1/c$	$P2_1/c$	$P2_1/c$	$P2_1/c$	$P2_1/c$	$P\bar{1}$
a/Å	12.581(3)	17.519(4)	9.5435(19)	9.5275(19)	10.169(2)	8.2582(17)
b/Å	12.583(3)	10.080(2)	14.915(3)	14.861(3)	16.396(3)	11.067(2)
c/Å	17.046(3)	22.931(5)	25.142(5)	25.048(5)	15.342(3)	14.080(3)
α/deg	90	90	90	90	90	93.68(3)
β/deg	93.32(3)	98.72(3)	97.06(3)	96.92(3)	96.09(3)	105.18(3)
γ/deg	90	90	90	90	90	92.97(3)
V/Å^3	2694.1(9)	4002.5(14)	3551.8(12)	3520.6(12)	2543.4(9)	1236.2(4)
Z	4	4	2	2	4	2
$2\theta_{max}$ (deg)	27.88	25.00	25.50	25.00	25.00	24.99
D_c/g·cm^{-3}	1.527	1.394	1.541	1.554	1.536	1.462
abs coeff/mm^{-1}	0.700	0.695	0.779	0.881	0.915	0.928
F(000)	1276	1730	1698	1704	1204	558
GOF	1.123	1.146	1.188	1.163	1.196	1.160
R_1 [$I > 2\sigma(I)$][a]	0.0479	0.0836	0.0700	0.0834	0.0720	0.0863
wR_2 (all data)[b]	0.1240	0.1887	0.1343	0.1545	0.1499	0.1787

[a] $R_1 = \Sigma||F_o| - |F_c||/\Sigma|F_o|$. [b] $wR_2 = [\Sigma w(F_o^2 - F_c^2)^2/\Sigma w(F_o^2)^2]^{1/2}$.

btmb = 4,4′-bis(1,2,4-triazol-1-ylmethyl)bipheny, H_3BTC = 1,3,5-benzenetricarboxylic acid, and H_2NDC = 1,2-benzenedicarboxylic acid. The structures and topological analyses of these complexes, along with the influence of the ligands, metal atoms, and pH values on the structures of the MOFs are represented and discussed. The thermal and catalytic properties of these complexes have also been investigated.

EXPERIMENTAL SECTION

Materials and Characterization. All chemicals were commercially available and used as purchased. Ligand 4,4′-bis(1,2,4-triazol-1-ylmethyl)biphenyl (btmb) was prepared according to the literature.[4c] IR data were recorded on a BRUKER TENSOR 27 spectrophotometer with KBr pellets in the region 400−4000 cm^{-1}. Elemental analyses (C, H, and N) were carried out on a Flash EA 1112 elemental analyzer. Powder X-ray diffraction (PXRD) patterns were recorded using Cu Kα1 radiation on a PANalytical X'Pert PRO diffractometer. Thermal analyses were performed on a Netzsch STA 449C thermal analyzer at the heating rate 10 °C·min^{-1} in air.

Synthesis of $\{[Co(btmb)(HBTC)]\cdot 2H_2O\}_n$ (1). A mixture of $CoCl_2\cdot 6H_2O$ (23.7 mg, 0.1 mmol), H_3BTC (21.0 mg, 0.1 mmol), btmb (31.6 mg, 0.1 mmol), and distilled water (10 mL) was placed in a 25 mL Teflon-lined stainless steel vessel, and then the pH value was adjusted to 5.0 by addition of methanolic $NaOCH_3$ solution. The mixture was sealed and heated at 130 °C for three days. After the mixture had been cooled to room temperature at a rate of 5 °C·h^{-1}, purple crystals of **1** were obtained with a yield of 70% (based on Co). Anal. Calcd for $C_{27}H_{24}CoN_6O_8$ (%): C, 52.35; H, 3.91; N, 13.57. Found: C, 52.30; H, 3.98; N, 13.52. IR (cm^{-1}, KBr): 3510s, 3447s, 3386s, 3143s, 3029w, 2979w, 1702s, 1629s, 1539s, 1454s, 1436s, 1374s, 1277s, 1200m, 1135m, 1109w, 1015m, 1014m, 988m, 938w, 898w, 874w, 842w, 801m, 758s, 719m, 677m, 651w.

Synthesis of $\{[Co_3(btmb)_3(BTC)_2(H_2O)_2]\cdot 6H_2O\}_n$ (2). Complex **2** was synthesized in a similar way as described for **1**, except that the pH value of the reaction was adjusted to 7.0 with methanolic $NaOCH_3$ solution. Purple crystals were obtained with a yield of 50% (based on Co). Anal. Calcd for $C_{72}H_{66}Co_3N_{18}O_{20}$ (%): C, 51.47; H, 3.96; N, 15.01. Found: C, 51.40; H, 4.00; N, 15.05. IR (cm^{-1}, KBr): 3426s, 3134m, 3021w, 1616s, 1561s, 1435m, 1366s, 1279m, 1208w, 1129m, 1092w, 10112m, 935w, 879w, 843w, 805w, 762m, 729m, 674m, 651w.

Synthesis of $\{[Co_3(btmb)_3(BTC)_2(H_2O)_4]\cdot 2H_2O\}_n$ (3). Complex **3** was synthesized in a similar way as described for **2**, except that the molar ratio of Co/H_3BTC/btmb is 3:1:1. Red block crystals of **3** were obtained with a yield of 45% (based on Co). Anal. Calcd for $C_{72}H_{66}Co_3N_{18}O_{18}$ (%): C, 52.47; H, 4.04; N, 15.30. Found: C, 52.40; H, 4.10; N, 15.28. IR (cm^{-1}, KBr): 3423s, 3130m, 3033w, 2934w, 1608s, 1558s, 1521s, 1424m, 1370s, 1276m, 1208w, 1129m, 1014m, 940w, 887w, 863w, 804m, 769m, 706m, 676m, 651w.

Synthesis of $\{[Ni_3(btmb)_3(BTC)_2(H_2O)_4]\cdot 2H_2O\}_n$ (4). Complex **4** was synthesized in a similar way as described for **2**, using $NiCl_2\cdot 6H_2O$ (23.7 mg, 0.1 mmol) instead of $CoCl_2\cdot 6H_2O$. Green crystals were obtained with a yield of 65% (based on Ni). Anal. Calcd for $C_{72}H_{66}Ni_3N_{18}O_{18}$ (%): C, 52.49; H, 4.04; N,15.30. Found: C, 52.66; H, 4.15; N, 15.16. IR (cm^{-1}, KBr): 3441s, 3134w, 1607s, 1559s, 1536s, 1425s, 1425m, 1370s, 1280m, 1209w, 1128m, 1017w, 886w, 861w, 802w, 770m, 727m, 711m, 675m, 652m.

Synthesis of $[Cu(btmb)(HBTC)]_n$ (5). A mixture of $Cu(NO_3)_2\cdot 3H_2O$ (24.1 mg, 0.1 mmol), btmb (31.6 mg, 0.1 mmol), H_3BTC (21.0 mg, 0.1 mmol), and 10 mL of distilled water was placed in a 25 mL Teflon-lined stainless vessel. The mixture was sealed and heated at 130 °C for three days. After the mixture had been cooled to room temperature at a rate of 5 °C·h^{-1}, blue crystals of **5** were obtained with a yield of 60% (based on Cu). Anal. Calcd for $C_{27}H_{20}CuN_6O_6$ (%): C, 55.15; H, 3.43; N, 14.29. Found: C, 54.97; H, 3.49; N, 14.02. IR (cm^{-1}, KBr): 3132m, 3036w, 1679s, 1614s, 1578m, 1528m, 1489w, 1427m, 1342s, 1248s, 1130s, 1105w, 1073w, 1024w, 1004m, 913w, 843m, 810w, 756s, 723s, 695s, 675m, 633w.

Synthesis of $[Cu(btmb)(NDC)]_n$ (6). Complex **6** was synthesized in a similar way as described for **5**, using H_2NDC (16.6 mg, 0.1 mmol)

dx.doi.org/10.1021/cg101494t |Cryst. Growth Des. 2011, 11, 2183–2193

Table 2. Selected Bond Lengths (Å) and Bond Angles (deg) for 1−6[a]

		Complex **1**			
Co(1)−O(1)	2.0301(15)	Co(1)−O(2)#1	2.0110(15)	Co(1)−O(3)#2	2.1221(15)
Co(1)−O(4)#2	2.2688(17)	Co(1)−N(1)	2.149(2)	Co(1)−N(6)#3	2.1468(19)
O(2)#1−Co(1)−O(1)	107.48(7)	O(2)#1−Co(1)−O(3)#2	95.56(7)	O(1)−Co(1)−O(3)#2	156.89(6)
O(2)#1−Co(1)−N(6)#3	93.52(8)	O(1)−Co(1)−N(6)#3	89.42(7)	O(3)#2−Co(1)−N(6)#3	87.37(7)
O(2)#1−Co(1)−N(1)	87.07(8)	O(1)−Co(1)−N(1)	89.92(7)	O(3)#2−Co(1)−N(1)	93.07(7)
N(6)#3−Co(1)−N(1)	179.23(8)	O(2)#1−Co(1)−O(4)#2	154.49(6)	O(1)−Co(1)−O(4)#2	97.62(6)
O(3)#2−Co(1)−O(4)#2	59.60(6)	N(6)#3−Co(1)−O(4)#2	91.12(7)	N(1)−Co(1)−O(4)#2	88.56(7)
		Complex **2**			
Co(1)−O(4)#1	2.015(3)	Co(1)−O(2)	2.032(4)	Co(1)−N(4)	2.053(5)
Co(1)−N(1)	2.057(5)	Co(2)−O(5)	2.031(4)	Co(2)−O(7)	2.155(4)
Co(2)−N(9)#3	2.163(7)	O(4)#1−Co(1)−O(2)	92.64(14)	O(4)#1−Co(1)−N(4)	111.83(16)
O(2)−Co(1)−N(4)	110.93(17)	O(4)#1−Co(1)−N(1)	109.30(16)	O(2)−Co(1)−N(1)	109.11(17)
N(4)−Co(1)−N(1)	119.69(18)	O(5)−Co(2)−O(5)#2	180.000(1)	O(5)−Co(2)−O(7)	91.91(18)
O(5)#2−Co(2)−O(7)	88.09(18)	O(7)−Co(2)−O(7)#2	180.0(3)	O(5)−Co(2)−N(9)#3	93.0(2)
O(5)#2−Co(2)−N(9)#3	87.0(2)	O(7)−Co(2)−N(9)#3	92.6(2)	O(7)#2−Co(2)−N(9)#3	87.4(2)
N(9)#3−Co(2)−N(9)#4	180.000(1)				
		Complex 3			
Co(1)−O(5)#1	2.040(3)	Co(1)−N(6)#2	2.113(4)	Co(1)−O(8)	2.113(3)
Co(1)−N(1)	2.146(4)	Co(1)−O(1)	2.154(3)	Co(1)−O(2)	2.215(3)
Co(2)−O(3)	2.046(3)	Co(2)−N(7)	2.146(4)	Co(2)−O(7)	2.156(3)
O(5)#1−Co(1)−N(6)#2	90.62(13)	O(5)#1−Co(1)−O(8)	90.81(12)	N(6)#2−Co(1)−O(8)	93.68(13)
O(5)#1−Co(1)−N(1)	87.97(13)	N(6)#2−Co(1)−N(1)	178.59(13)	O(8)−Co(1)−N(1)	86.38(13)
O(5)#1−Co(1)−O(1)	99.24(10)	N(6)#2−Co(1)−O(1)	93.69(12)	O(8)−Co(1)−O(1)	167.46(12)
N(1)−Co(1)−O(1)	86.50(13)	O(5)#1−Co(1)−O(2)	159.49(10)	N(6)#2−Co(1)−O(2)	89.18(12)
O(8)−Co(1)−O(2)	109.67(11)	N(1)−Co(1)−O(2)	92.13(12)	O(1)−Co(1)−O(2)	60.33(10)
O(3)#3−Co(2)−O(3)	180.000(1)	O(3)−Co(2)−N(7)#3	89.94(12)	O(3)−Co(2)−N(7)	90.06(12)
N(7)#3−Co(2)−N(7)	180.000(1)	N(7)−Co(2)−O(7)#3	88.88(13)	O(3)#3−Co(2)−O(7)	86.28(11)
O(3)−Co(2)−O(7)	93.72(11)	N(7)−Co(2)−O(7)	91.12(13)	O(7)#3−Co(2)−O(7)	180.000(1)
		Complex **4**			
Ni(1)−O(5)	2.019(3)	Ni(1)−N(6)#1	2.073(5)	Ni(1)−O(7)	2.073(4)
Ni(1)−N(1)	2.090(5)	Ni(1)−O(3)#2	2.107(3)	Ni(1)−O(4)#2	2.183(3)
Ni(2)−O(1)	2.031(3)	Ni(2)−N(9)	2.092(5)	Ni(2)−O(8)	2.113(4)
O(5)−Ni(1)−N(6)#1	90.25(16)	O(5)−Ni(1)−O(7)	91.96(14)	N(6)#1−Ni(1)−O(7)	93.30(16)
O(5)−Ni(1)−N(1)	87.80(17)	N(6)#1−Ni(1)−N(1)	178.02(18)	O(7)−Ni(1)−N(1)	87.11(16)
O(5)−Ni(1)−O(3)#2	98.27(13)	N(6)#1−Ni(1)−O(3)#2	92.43(15)	O(7)−Ni(1)−O(3)#2	168.25(14)
N(1)−Ni(1)−O(3)#2	87.52(16)	O(5)−Ni(1)−O(4)#2	159.61(13)	N(6)#1−Ni(1)−O(4)#2	90.16(16)
O(7)−Ni(1)−O(4)#2	108.37(14)	N(1)−Ni(1)−O(4)#2	91.55(16)	O(3)#2−Ni(1)−O(4)#2	61.34(12)
O(5)−Ni(1)−C(32)#2	128.70(16)	O(1)#3−Ni(2)−O(1)	180.00(14)	O(1)−Ni(2)−N(9)#3	90.27(16)
O(1)−Ni(2)−N(9)	89.73(16)	N(9)#3−Ni(2)−N(9)	180.0	O(1)#3−Ni(2)−O(8)	94.13(14)
O(1)−Ni(2)−O(8)	85.87(14)	N(9)#3−Ni(2)−O(8)	89.32(16)	N(9)−Ni(2)−O(8)	90.68(16)
O(8)−Ni(2)−O(8)#3	180.000(1)				
		Complex **5**			
Cu(1)−O(4)#1	1.966(3)	Cu(1)−O(1)	1.969(3)	Cu(1)−N(4)	1.975(4)
Cu(1)−O(5)#2	2.366(3)	Cu(1)−N(1)	1.975(4)	O(4)#1−Cu(1)−O(1)	156.58(13)
O(4)#1−Cu(1)−N(4)	88.21(15)	O(1)−Cu(1)−N(4)	89.79(14)	O(4)#1−Cu(1)−N(1)	91.75(14)
O(1)−Cu(1)−N(1)	90.99(14)	N(4)−Cu(1)−N(1)	178.13(15)	O(4)#1−Cu(1)−O(5)#2	107.16(12)
O(1)−Cu(1)−O(5)#2	96.01(11)	N(4)−Cu(1)−O(5)#2	86.75(14)	N(1)−Cu(1)−O(5)#2	91.47(13)
		Complex **6**			
Cu(1)−O(1)	1.961(4)	Cu(1)−N(1)	2.002(5)	Cu(2)−O(3)	1.956(4)
Cu(2)−N(4)	1.976(6)	O(1)#1−Cu(1)−O(1)	180.00(17)	O(1)#1−Cu(1)−N(1)	90.3(2)

dx.doi.org/10.1021/cg101494t |*Cryst. Growth Des.* 2011, 11, 2183–2193

Table 2. Continued

Complex **1**					
O(1)−Cu(1)−N(1)	89.7(2)	N(1)#1−Cu(1)−N(1)	180.000(2)	O(3)−Cu(2)−O(3)#2	180.000(1)
O(3)−Cu(2)−N(4)#2	91.7(2)	O(3)−Cu(2)−N(4)	88.3(2)	N(4)#2−Cu(2)−N(4)	180.000(1)

[a] Symmetry transformations used to generate equivalent atoms in complex **1**: (#1) $-x+1, -y+1, -z+2$; (#2) $-x+1, y-{}^1/_2, -z+{}^3/_2$; (#3) $x+1, y+1, z$. Complex **2**: (#1) $x, y-1, z$; (#2) $-x+2, -y+1, -z+1$; (#3) $x+1, -y+{}^1/_2, z-{}^1/_2$; (#4) $-x+1, y+{}^1/_2, -z+{}^3/_2$. Complex **3**: (#1) $-x+2, y-{}^1/_2, -z+{}^1/_2$; (#2) $x+1, y+1, z$; (#3) $-x+2, -y+1, -z+1$. Complex **4**: (#1) $x+1, y-1, z$; (#2) $-x+2, y-{}^1/_2, -z+{}^1/_2$; (#3) $-x+2, -y+2, -z$. Complex **5**: (#1) $x-1, y, z$; (#2) $-x, y-{}^1/_2, -z+{}^1/_2$. Complex **6**: (#1) $-x+1, -y, -z+2$; (#2) $-x+1, -y, -z+1$.

instead of H_3BTC. Deep blue crystals of **6** were obtained with a yield of 52% (based on Cu). Anal. Calcd for $C_{26}H_{20}CuN_6O_4$ (%): C, 57.40; H, 3.71; N, 15.45. Found: C, 57.01; H, 3.65; N, 15.42. IR (cm^{-1}, KBr): 3118m, 3037w, 1605s, 1574s, 1533m, 1443w, 1369s, 1281m, 1215w, 1128m, 1081w, 1006m, 835w, 805w, 757m, 704w, 673w, 650w.

Crystal Structure Determination. The data of the six complexes were collected on a Rigaku Saturn 724 CCD diffractomer (Mo Kα, λ = 0.71073 Å) at the temperature 20 ± 1 °C. Absorption corrections were applied by using a multiscan program. The data were corrected for Lorentz and polarization effects. The structures were solved by direct methods and refined with a full-matrix least-squares technique based on F^2 with the SHELXL-97 crystallographic software package.[6] The hydrogen atoms were assigned with common isotropic displacement factors and included in the final refinement by using geometrical restraints. But the hydrogen atoms of water molecules for **3** and **4** were located from difference Fourier maps and refined with isotropic displacement parameters. Crystallographic crystal data and structure processing parameters for complexes **1**−**6** are summarized in detail in Table 1. Selected bond lengths and bond angles are listed in Table 2.

Experimental Procedure for the Catalytic Oxidative Coupling of DMP[7]. One mmol of DMP (122 mg) was dissolved in 3 mL of water containing 1 mmol of NaOH (40 mg) and 0.1 mmol of sodium *n*-dodecyl sulfate (SDS) (29 mg). 0.01 mmol of complex with appropriate size was added to the above solution, and the mixture was stirred at 50 °C. Then, 10 μL of H_2O_2 (30% aqueous solution) was slowly added into the mixture using a microinjector every 15 min (2 times in all). After 8 h, the reaction was stopped and 1.17 g of NaCl was added. Then the mixture was transferred into a separatory funnel, and the organic materials were extracted with $CHCl_3$ 3 times. The combined organic extracts were dried with anhydrous $MgSO_4$, and the filtrate was evaporated in vacuo. The products were separated by preparative TLC performed on dry silica gel plates with ethylether/petroleum ether (1:3 v/v) as the developing solvent. The main product, poly(1,4-phenylene ether) (PPE), and byproduct, diphenoquinone (DPQ), were collected and dried in vacuo, repectively.

PPE: ^{1}H NMR (400 MHz, $CDCl_3$) δ: 2.10 (s, 6H), 6.44 (s, 2H). ^{13}C NMR (100 MHz, $CDCl_3$) δ: 16.3−16.8, 114.1, 114.5, 124.4, 124.9, 128.6, 129.0, 131.6, 132.7, 145.6, 146.4, 151.4, 152.2, 154.5, 154.7. IR (cm^{-1}, KBr): 3429m, 1607s, 1470s, 1306s, 1188s, 1022s, 858m.

RESULTS AND DISCUSSION

Syntheses of the Complexes. Hydrothermal synthesis is a relatively complicated process, and the final products are often unpredictable under a given set of conditions. The reaction variables (metal ions, pH value, metal−ligand ratio, temperature, etc.) may affect the final products remarkably. In our system, the central metals, pH value, and metal−ligand ratio play important roles in the formation of new complexes. For preparation of complexes **1**−**3**, the raw materials are the same, but distinct structures are obtained for the different pH values or molar ratio of Co/H_3BTC/btmb. However, in the syntheses of complexes **4** and **5**, when the same reaction conditions used to prepare complexes **1**−**3** were performed on Ni or Cu salts, we only obtained one complex for each kind of metal ions, respectively. That is to say, cobalt(II) ion is relatively sensitive to the reaction conditions. For preparation of complex **6**, the reaction condition used in the Experimental Section is the best choice. If the pH value or the molar ratio of reagents was changed, no crystals were obtained. All of the complexes **1**−**6** are stable in air and are insoluble in water and common organic solvents such as ethanol, benzene, acetone, and acetonitrile. In the IR spectra of complexes, the characteristic bands attributed to the protonated carboxylate groups are observed at 1702 cm^{-1} for **1** and 1679 cm^{-1} for **5**, respectively, indicating the incomplete deprotonation of H_3BTC. The absence of such bands in other complexes indicates the complete deprotonation of aromatic multicarboxylate. This is in agreement with the result of X-ray single-crystal analysis.

Crystal Structure of $\{[Co(btmb)(HBTC)]\cdot 2H_2O\}_n$ (1). Complex **1** crystallizes in the monoclinic space group $P2_1/c$. Each Co(II) atom exhibits a distorted octahedral environment, the equatorial plane of which comprises four carboxylate oxygen atoms from three distinct $HBTC^{2-}$ anions and two nitrogen atoms from two btmb ligands occupying the apical site (Figure 1a). The Co−O/N distances are in the range 2.0104−2.2690 Å, which are in the normal range of those observed in cobalt complexes.[8] The incompletely deprotonated $HBTC^{2-}$ ligand acts as a μ_3-bridge linking three Co(II) atoms, in which one carboxylate group adopts the bidentate chelate mode and the other adopts a μ_2-η^1:η^1 fashion (type I in Scheme 1).

Further, the Co(II) atoms are in turn connected by $HBTC^{2-}$ to give rise to a two-dimensional (2D) sheet structure along the *bc* plane (Figure 1b). The architecture of the 2D sheet is based on a dinuclear unit $[Co_2(COO)_2]$ with a Co···Co distance of 4.474 Å. The sheets are pillared by ligand btmb in a *trans* conformation[9] via the Co−N connections to generate a pillar-layered three-dimensional (3D) framework. Better insight into such an elegant framework can be accessed by the topology method. In **1**, the dinuclear unit $[Co_2(COO)_2]$ acts as nodes, and the btmb serves as linkers; therefore, the combination of nodes and linkers suggests the 6-connected framework with a Schläfli symbol of $4^4\cdot 6^{10}\cdot 8$. Careful inspection of such a framework suggests that the net is self-penetrating. As shown in Figure 1c, each six-membered shortest circuit is catenated by two rods of the same network.[10] Self-penetration is an unusual form of topological entanglement. Thus, **1** can be considered as another example of the self-penetrated coordination polymers.[11]

Crystal Structure of $\{[Co_3(btmb)_3(BTC)_2(H_2O)_2]\cdot 6H_2O\}_n$ (2). As depicted in Figure 2a, there are two types of coordination environments around the Co(II) atoms in the structure of **2**. It can be clearly seen that the Co1 atom is 4-coordinated, with a slightly distorted tetrahedral geometry, by two oxygen atoms from two different BTC^{3-} anions and two nitrogen atoms from two btmb ligands. The Co−O bond lengths are 2.015(3) and

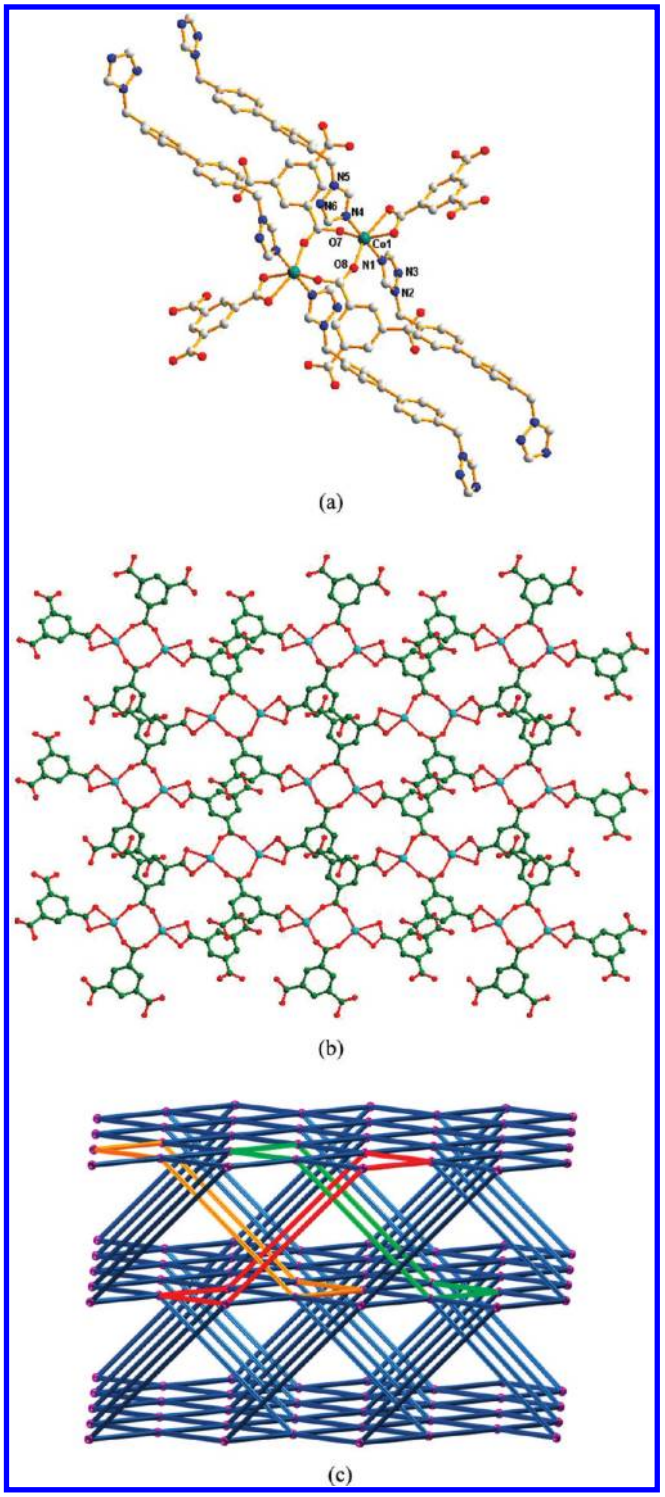

Figure 1. (a) Coordination environment around the Co(II) centers in **1**. (b) The 2D sheet structure constructed from Co(II) centers and $HBTC^{2-}$ anions. (c) Schematic representation of $4^4 \cdot 6^{10} \cdot 8$ topology of complex **1** and the self-penetrated shortest circuits (green, orange, and red).

2.032(4) Å, respectively; the Co−N bond lengths are 2.053(5) and 2.057(5) Å, respectively. Co2 adopts a distorted octahedral CoO_4N_2 coordination geometry completed by two carboxylate oxygen atoms from two BTC^{3-} anions (Co−O 2.031(4) Å), two terminal water molecules (Co−O 2.155(4) Å), and two nitrogen atoms from two btmb ligands (Co−N 2.163(7) Å). Each completely deprotonated BTC^{3-} ligand displaying the tri(monodentate) coordinated mode (II), as illustrated in Scheme 1, coordinates to three Co(II) centers. Then the Co(II) cations are bridged by the BTC^{3-} anions to form a one-dimensional (1D) ladder structure (Figure 2b).

The btmb ligands in **2** adopt two kinds of conformations. One takes the *cis* conformation,[12] which links one Co2 atom (at the ladder center) and one Co1 atom (at the other ladder side) with a Co2···Co1 distance of 15.00(40) Å (Figure 2c, pink ones). These Co1 and Co2 atoms are in the same Co−BTC layer, while the other btmb molecule in the *trans* conformation links Co1 atoms between adjacent layers with a distance of 17.75(42) Å (blue ones in Figure 2c). These links give rise to the complicated 3D framework as shown in topological Figure 2d.

Topological analysis was carried out to get insight into the structure of **2**. If Co1 and Co2 are simplified as two kinds of four-connected nodes, and the btmb and BTC^{3-} ligands are defined as 2- and 3-connected nodes, respectively, the 3D framework of **2** can be described as a trinodal (3,4)-connected topology with the Schläfli symbol $(6^2 \cdot 8^4)(6^4 \cdot 8^2)(6^3)$.

Crystal Structures of $\{[Co_3(btmb)_3(BTC)_2(H_2O)_4] \cdot 2H_2O\}_n$ (3) and $\{[Ni_3(btmb)_3(BTC)_2(H_2O)_4] \cdot 2H_2O\}_n$ (4). Similar cell parameters with the same space group $P2_1/c$ (Table 1) and the results of crystallographic analyses confirm that **3** and **4** are isostructural. Thus, only the structure of **3** is described in detail as a typical example, while the structure of **4** is provided in the Supporting Information (Figure S1).

As shown in Figure 3a, there are two independent cobalt atoms: Co1 is coordinated by three BTC^{3-} oxygen atoms, two btmb nitrogen atoms, and one water molecule to give the CoO_4N_2 distorted octahedral geometry, and Co2 also shows the CoO_4N_2 octahedral geometry but completed by two BTC^{3-} oxygen atoms, two btmb nitrogen atoms, and two water molecules. The Co−O/N bond lengths are in the range 2.040(3)−2.215(3) Å. All of the coordination bonds are within normal distances.[13] In **3**, each completely deprotonated BTC^{3-} serves as a 3-connected node to coordinate with three Co(II) atoms with the coordination mode of type III, as illustrated in Scheme 1, generating a 2D extended network (Figure 3b). In the network, six Co(II) atoms are bridged by six BTC^{3-}, forming a macrocyclic ring in which the separations of the opposite metal atoms are 10.149, 14.915, and 26.014 Å, respectively.

These 2D layers are further connected by two types of btmb ligands acting as bridging pillars to build a 3D layer pillar framework. Both types of the btmb ligands adopt *trans* conformation with different $N_{donor}-C_{sp3}\cdots C_{sp3}-N_{donor}$ torsion angles (180° for the centrosymmetric ligands and 174.1° for the noncentrosymmetric ones). As shown in Figure 3c, if Co1 and Co2 are simplified as two kinds of four-connected nodes, and the btmb and BTC^{3-} ligands are defined as a 2- and 3-connected nodes, respectively, the 3D framework of **3** can be described as a trinodal (3,4)-connected topology with Schläfli symbol of $(6^2 \cdot 8 \cdot 10^3)(6^4 \cdot 8 \cdot 10)(6 \cdot 10^2)$.

Crystal Structure of $[Cu(btmb)(HBTC)]_n$ (5). Single crystal structure analysis reveals that complex **5** is also a pillar-layered 3D framework, which is similar to the reported structure $\{[Cu_4(BTC)_4(btmb)_4] \cdot H_2O\}_n$.[4e] But there are no lattice water molecules in complex **5**. As shown in Figure 4a, each Cu(II) atom is five coordinated by two nitrogen atoms of two btmb ligands and three oxygen atoms from three $HBTC^{2-}$ anions, taking a distorted square-pyramidal coordination environment ($\tau = 0.36$).[14]

Scheme 1. Coordinated Mode of the H_3BTC Ligand

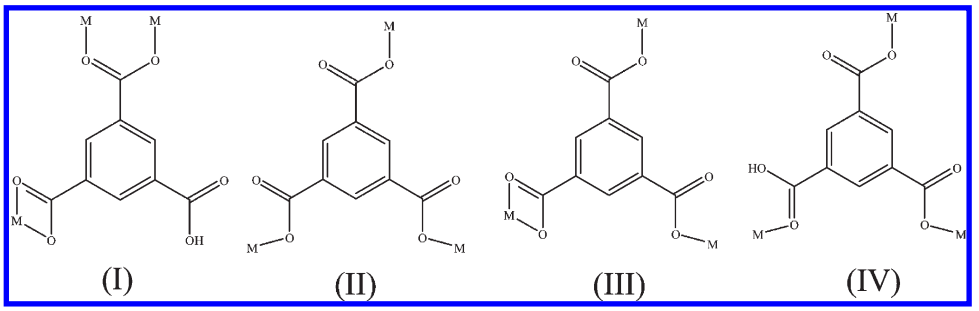

The Cu−N bond lengths are 1.975(4) Å, and the Cu−O bond lengths are in the range 1.966(3)−2.366(3) Å, which are comparable to those observed for $\{[Cu(btp)(HBTC)_2]\cdot 0.5H_2O\}_n$ (btp = 1,3-bis(1,2,4-triazol-1-yl)propane).[15] Each incompletely deprotonated $HBTC^{2-}$ ligand serves as a three-connected node to coordinate with three Cu(II) atoms through its three carboxylates in monodentate mode (type IV), generating a 2D (6,3) network, as shown in Figure 4b. Then the 2D layers are further connected by two kinds of btmb ligands, forming a 3D layer pillar framework (Figure 4c). Both kinds of btmb ligands adopt a *trans* conformation with a $N_{donor}-C_{sp3}\cdots C_{sp3}-N_{donor}$ torsion angle of 180°. Though both kinds of btmb have the same conformation with torsion angles of 180°, the $N_{donor}\cdots N-C_{sp3}\cdots C_{sp3}$ torsion angles in these two kinds of btmb ligands are different. The torsion angles are 5.990° for N1 containing btmb (with $N_{donor}\cdots N_{donor}$ 12.81 Å) or 6.248° for N4 containing btmb (with $N_{donor}\cdots N_{donor}$ 13.15 Å), which leads to the different Cu···Cu distances (14.19 Å or 14.93 Å) separated by these two kinds of btmb.

To further understand the structure of the complex, topological analysis was performed on **5**. As discussed above, each $HBTC^{2-}$ and btmb ligand links three and two Cu(II) atoms, respectively; accordingly, the $HBTC^{2-}$ and btmb can be regarded as 3- and 2-connected nodes, respectively. As for each Cu(II) atom, it links three $HBTC^{2-}$ and two btmb ligands; hence, the Cu(II) atom can be treated as a 5-connector. According to the simplification principle, the resulting structure of complex **5** is a binodal (3,5)-connected gra net with a Schläfli symbol $(6^3)(6^9\cdot 8)$.

Crystal Structure of [Cu(btmb)(NDC)]$_n$ (6). Compared with complex **5**, the tricarboxylic acid H_3BTC ligand is replaced by dicarboxylate ligand H_2NDC, and a structurally different complex **6** was successfully isolated. In the asymmetry unit (Figure 5a), there are two independent Cu(II) atoms, but both of them have the same coordination environment: Cu1 and Cu2 are four-coordinated by two nitrogen atoms from two btmb ligands (Cu1−N1 2.002(5) Å, Cu2−N4 1.976(6) Å) and two oxygen atoms from two NDC^{2-} anions (Cu1−O1 1.961(4) Å, Cu2−O3 1.956(4) Å) in a distorted square planar coordination geometry. Each NDC^{2-} ligand adopting a μ^2-η^1:η^1 bridging mode coordinates to symmetry-related Cu1 and Cu2 atoms to generate a 1D zigzag chain with the Cu···Cu distance of 7.040 Å (Figure 5b). These 1D chains are then linked by two kinds of btmb ligands via Cu−N coordination bonds, thus leading to the formation of a 3D framework. Both kinds of btmb ligands adopt the same conformation with the same $N_{donor}-C_{sp3}\cdots C_{sp3}-N_{donor}$ torsion angles to that of **5**. The $N_{donor}\cdots N-C_{sp3}\cdots C_{sp3}$ torsion angles are 105.0° for N1 containing btmb (with $N_{donor}\cdots N_{donor}$ 15.10 Å and Cu···Cu 18.46 Å) and 90.18° for N4 containing btmb (with $N_{donor}\cdots N_{donor}$ 14.58 Å and Cu···Cu 17.28 Å), respectively. Better insight into the present 3D framework can be accessed by the topological method. Each Cu(II) atom connects to four other Cu(II) atoms via two NDC^{2-} and two btmb spacers; hence, the Cu(II) atoms can be viewed to be 4-connected nodes. Such connectivity repeats infinitely to give the 3D framework with $(6^5\cdot 8)_2$ topology (Figure 5c).

Coordination of Aromatic Multicarboxylate Ligands and Bis(triazole) Ligand. In complexes **1**−**5**, H_3BTC ligand is completely or partially deprotonated under different pH values and consequently exhibits rich coordination modes. Thus, several metal-(H)BTC skeletons (1D ladder, 2D layer) are formed. In **1**, each incompletely deprotonated $HBTC^{2-}$ ligand coordinates to three Co(II) centers, and the Co(II) centers are connected by $HBTC^{2-}$ anions to form a 2D network. For **2**, every BTC^{3-} anion coordinates to three Co(II) centers, and Co(II) centers are bridged by BTC^{3-} anions to form a 1D ladder skeleton. In the structures of **3** and **4**, each BTC^{3-} also coordinates to three M(II) (M = Co or Ni) centers, and the M(II) centers are linked by BTC^{3-} to form a 2D polymeric layer, respectively. In the case of **5**, the $HBTC^{2-}$ anion coordinates to three Cu(II) centers, and the Cu(II) centers are connected by $HBTC^{2-}$ anions to furnish a 2D honeycomb network. When H_3BTC ligand was replaced by ligand H_2NDC, complex **6** was obtained. Each NDC^{2-} ligand in **6** coordinates to two Cu(II) centers to generate a 1D zigzag chain. From the discussion above, the result shows that the coordination mode of the carboxylate group has an important influence on the networks constructed by carboxylate ligands and metal centers.

In this study, complexes **1**−**6** display a diversity of 3D frameworks, and the connectivities of the six complexes are strongly related to the bis(triazole) ligands. In these structures, the ligand btmb utilizes two exo-N atoms of the triazole units to coordinate to the metal centers just like a linker. As a result, the 1D or 2D structures constructed by metal centers and aromatic multicarboxylate ligands are connected by ligands btmb to generate 3D frameworks with versartile topologies. The existence of long flexible ligand btmb not only promotes higher dimensionality but also favors the formation of peculiar motifs. For example, in **1**, the 2D Co(II)-$HBTC^{2-}$ layer is pillared by btmb to generate a pillar-layered 3D framework with the self-penetrating topology.

The mixed polycarboxylate and N donor ligands have been proven to be a useful building block in construction of MOFs with novel structures and unique properties. For example, the Mn(II) and Co(II) frameworks with BTC^{3-} and bimb ligands are among the rare examples of MOFs that exhibit high

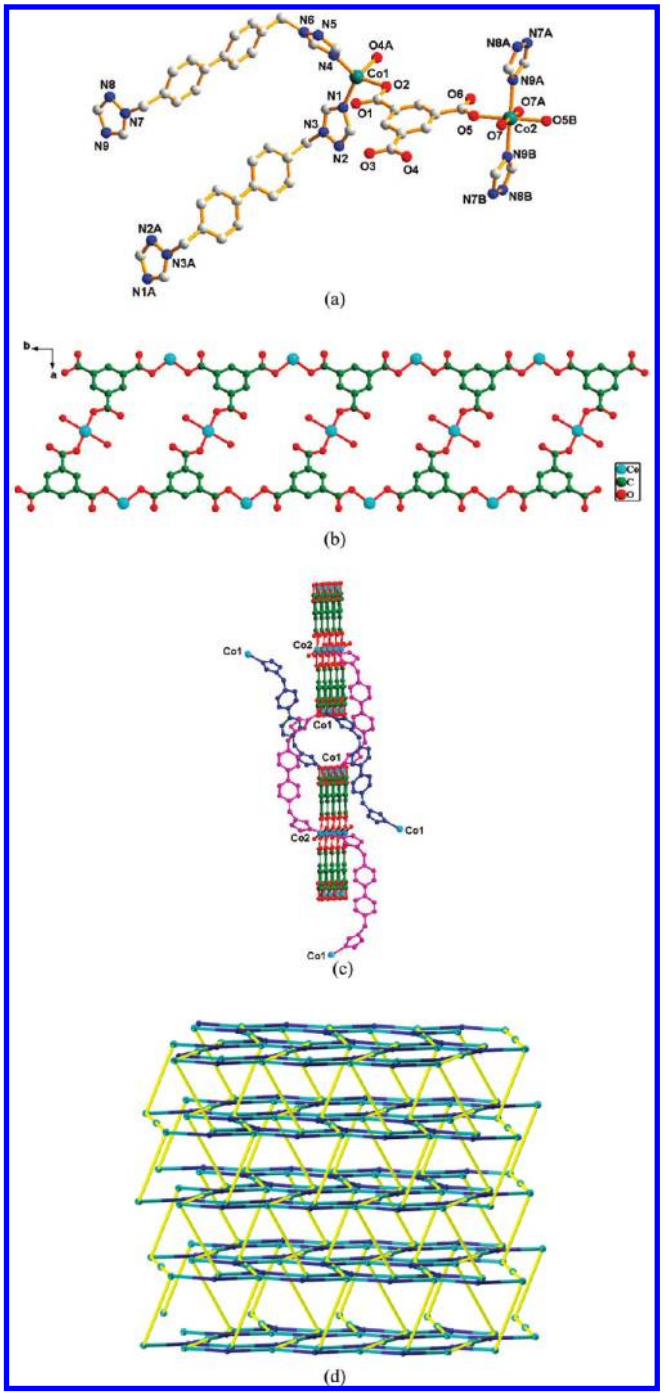

Figure 2. (a) Coordination environments around the Co(II) centers in **2**. Hydrogen atoms and solvent molecules are omitted for clarity. (b) View of the $[Co_3(BTC)_2]_n$ ladder. (c) Different conformations of btmb ligands in **2**. (d) Schematic representation of trinodal (3,4)-connected topology with the topological notation $(6^2 \cdot 8^4)(6^4 \cdot 8^2)(6^3)$. Color code: sea-green ball, 4-connected Co(II) node; blue ball, 3-connected BTC^{3-} node; yellow stick, 2-connected btmb ligand.

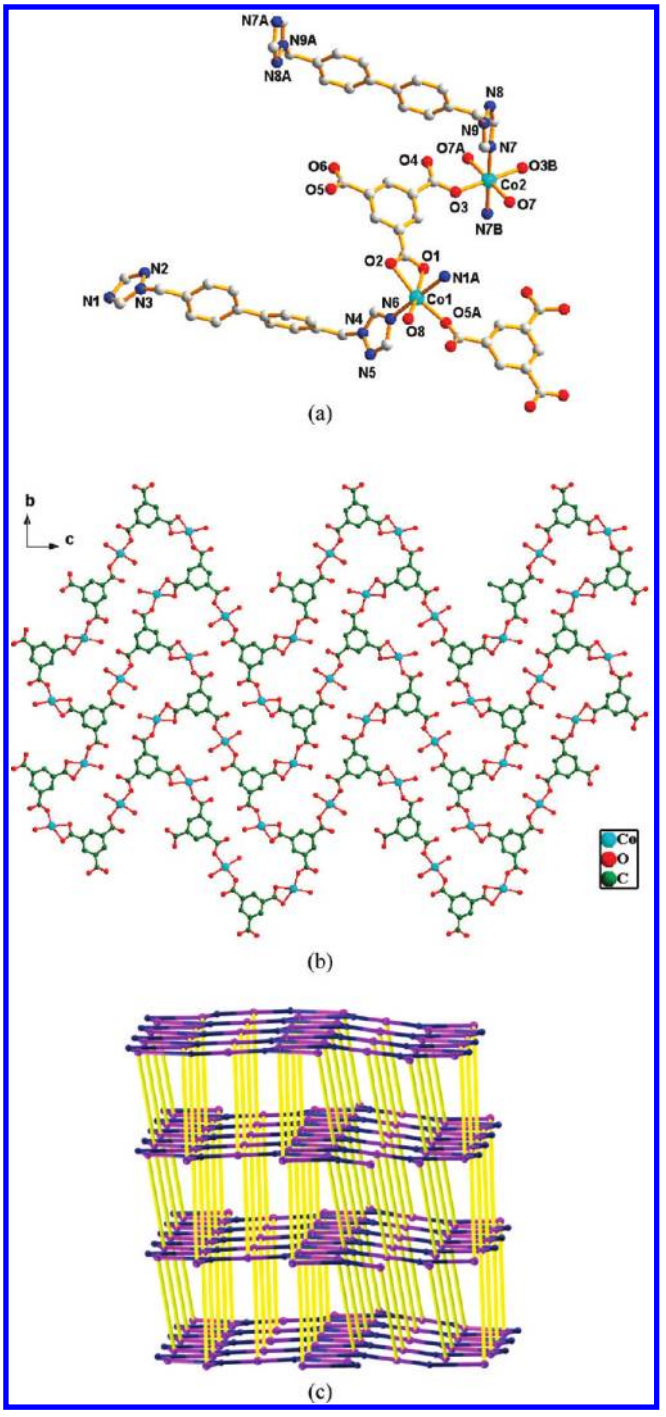

Figure 3. (a) Coordination environments around the Co(II) centers in **3**. Hydrogen atoms and solvent molecules are omitted for clarity. (b) The 2D sheet structure constructed from Co(II) centers and BTC^{3-} anions. (c) The 3D layer pillar framework of **3**. Color code: purple ball, 4-connected Co(II) node; blue ball, 3-connected BTC^{3-} node; yellow stick, 2-connected btmb ligand.

photocatalytic activity for dye degradation under UV light (H_3BTC = 1,3,5-benzenetricarboxylic acid and bimb = 4,4′ -bis-(1-imidazolyl)biphenyl),[16] and the Ni(II) framework with *m*-BTC^{3-} and bpy containing beautiful "S" ribbons shows very interesting ferromagnetic properties (*m*-H_3BTC = 1,2,4-benzenetricarboxylic acid and bpy = 4,4′-bipyridine).[17] A systematic study was carried out in this work by aromatic multicarboxylate ligands, and MOFs with different structures and topologies were obtained. The results of this work provide a nice example of the construction of MOFs using a mixed ligand strategy. On the other hand, many factors, such as the stoichiometric ratio of the components, the pH value, and the versatility of the metal

dx.doi.org/10.1021/cg101494t |*Cryst. Growth Des.* 2011, 11, 2183–2193

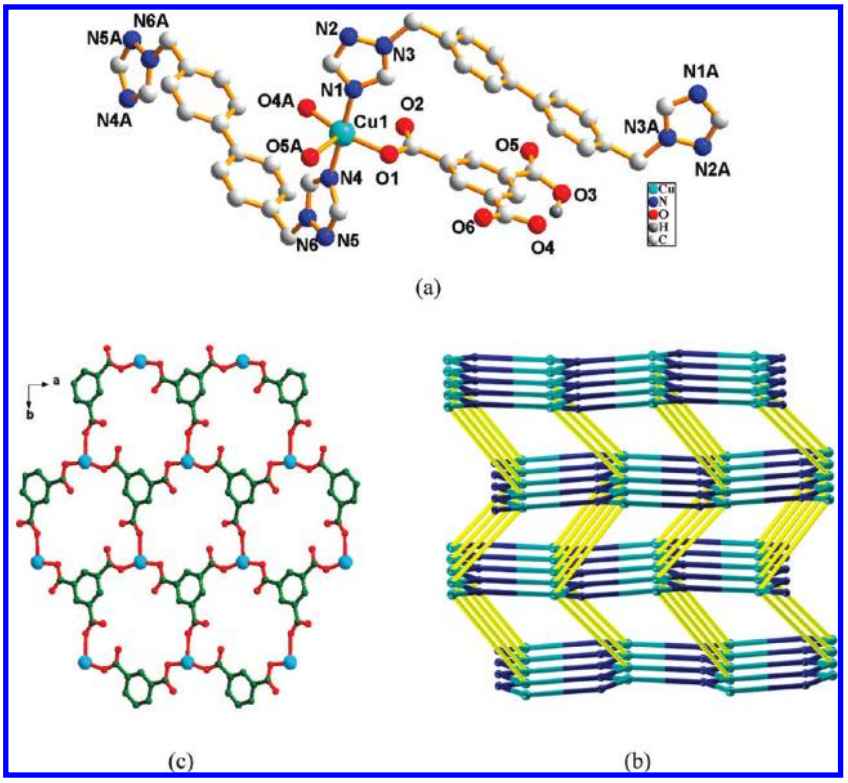

Figure 4. (a) Coordination environments around the Cu(II) centers in **5**. (b) Infinite 2D (6,3) network constructed from Cu(II) ions coordinated to $HBTC^{2-}$ ligands. (c) Schematic representation of binodal (3,5)-connected topology with the topological notation $(6^3)(6^9 \cdot 8)$. Color code: sea-green ball, 5-connected Cu(II) node; blue ball, 3-connected $HBTC^{2-}$ node; yellow stick, 2-connected btmb ligand.

coordination geometries and reaction conditions, can influence the formation of the final products. So it is still a challenge to obtain the desired MOFs.

Thermal Analyses. To estimate the stability of the coordination architectures, thermogravimetric analyses (TGA) were carried out (Figure 6). The phase purities of the bulk samples were identified by powder X-ray diffraction (Figures S2 in the Supporting Information). The TGA curve of **1** shows the first step weight loss (2.91%) at 73.8−124.5 °C, corresponding to the loss of a lattice water molecule (calcd: 3.42%), and after that, from 124.5−349.5 °C, the second step weight loss (2.91%), corresponding to the loss of the other lattice water molecule (calcd: 2.70%). The removal of the organic components occurs in the range 349.5−495.0 °C. The remaining weight corresponds to the formation of Co_2O_3 (obsd, 13.2%; calcd, 13.3%). For **2**, the first step weight loss, attributed to the gradual release of six lattice water molecules and two coordinated water molecules, is observed in the range 84.5−317.5 °C (obsd, 8.70%; calcd, 8.58%). The second step weight loss from 317.4 to 466.3 °C corresponds to the decomposition of btmb and BTC^{3-}, leading to the formation of Co_2O_3 as the residue (obsd, 14.81%; calcd, 16.87%). As for complexes **3** and **4**, the initial weight losses in the range 133.8−283.9 °C and 111.75−305.9 °C correspond to the losses of the two lattice water and four coordinated water molecules (For **3**: obsd, 6.85%; calcd, 6.56%. For **4**: obsd, 7.24%; calcd, 6.56%), respectively. The further weight losses represented the decomposition of the anhydrous compounds, leading to the formation of a brown black residue of Co_2O_3 (obsd, 14.40%; calcd, 15.09%) and a black residue of NiO (obsd, 12.42%; calcd, 13.46%), respectively. The TGA data of complex **5** show that it is stable up to 308 °C and then keeps losing weight from 308 to 497 °C, corresponding to the losses of btmb and the decomposition of the $HBTC^{2-}$. A black amorphous residue of CuO (observed 13.42%, calculated 12.57%) is remained. The TGA curve of complex **6** exhibits that it is stable up to 246 °C and then loses weight from 246 to 606 °C, corresponding to the decomposition of btmb and NDC^{2-}. The remaining weight corresponds to the formation of CuO (obsd, 14.51%; calcd, 14.86%).

Catalytic Properties of the MOFs. MOFs as catalysts have attracted increasing attention, motivated by many inherent advantages, such as the controlled oxidation state of the cation, the possibility to tune the electron density on the metal as a contribution of different ligands, multiactive metal centers available within the molecule, as well as controlled texture (pore size and shape) that may induce some shape selectivity effects.[18] Then we investigated the catalytic activities of complexes **1**−**6** in oxidative coupling reaction of 2,6-dimethylphenol (DMP). The main product of this reaction, poly(1,4-phenylene ether) (PPE), is a high-performance engineering plastic with outstanding chemical and physical properties.[19] In this paper we select the green oxidative coupling reaction system of DMP in water with clean oxidant H_2O_2 (Scheme S1 in the Supporting Information). Under the same reaction conditions, complexes **1**−**6** show different catalytic activities. The catalytic data are summarized in Table 3. On the basis of the above experimental results and previous literature,[20] a plausible reaction mechanism for the present oxidative coupling reaction was proposed as follows: DMP is dissolved in the basic aqueous phase to form the phenolate anion; these phenoxide anions coordinate to M(II) centers, and then electron transfers from the coordinated phenoxide anions to M(II) ions occur, leading to the formation of

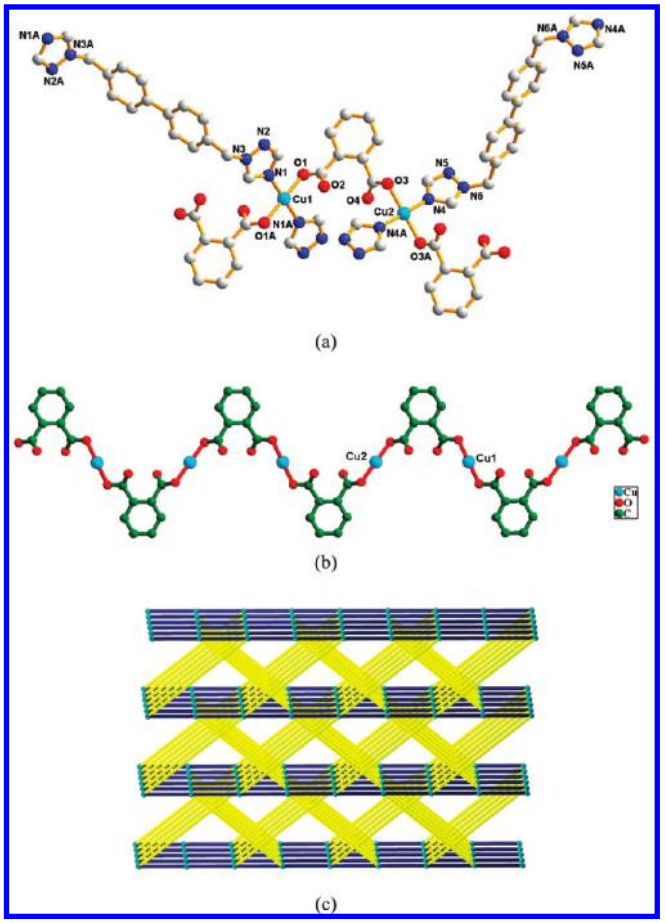

Figure 5. (a) Coordination environments around the Cu(II) centers in **6**. Hydrogen atoms are omitted for clarity. (b) Infinite zigzag chain constructed from Cu(II) ions coordinated to NDC^{2-} ligands. (c) Topological representation of the 4-connected topology with the topological notation $(6^5 \cdot 8)_2$. Color code: sea-green ball, 4-connected Cu(II) node; blue stick, 2-connected NDC^{2-} ligand; yellow stick, 2-connected btmb ligand.

phenoxyl radicals. The resultant M(I) ions were reoxidized to M(II) ions by H_2O_2 (M = Cu, Co, or Ni). The C−O coupling of these phenoxyl radicals yields the linear polymer PPE; the C−C coupling of these phenoxyl radicals results in the byproduct DPQ (Scheme S2 of the Supporting Information).

All the complexes have a 3D porous framework; however, the catalytic activities of these complexes possess big differences. From Table 3, we found that complexes **5** and **6** show better activities than complexes **1**−**4** in this system. The results indicated that Cu(II)-containing complexes have good catalytic activities in the oxidative coupling reaction. The contrasting reaction using $CuCl_2$ as catalyst only gives trace amounts of PPE. The reason is that the N/O donor ligands interact with metal ions to provide a delocalized electronic system within complexes, which induce the modification of the electronic properties of the molecules. This favors the coordination of DMP to metal centers to form the proposed active metal species and the subsequent polymerization of DMP.[18f,21] Likewise, Reedijk and co-workers have also shown that a series of Cu(II) complexes incorporating structurally related N,O-containing ligands underwent this polymerization more efficiently than copper(II) salts.[22] This suggests that the copper

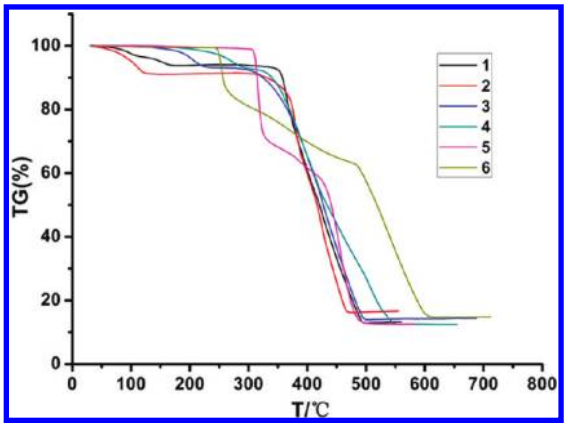

Figure 6. TG plots of these MOFs.

Table 3. Catalytic Activities of Complexes 1−6 for Oxidative Polymerization of DMP[a]

catalyst	conversion of DMP (%)	yield (%)[b] PPE	selectivity[c] of PPE (%)
1	60	32	54
2	75	44	64
3	54	25	78
4	56	21	63
5	97	88	78
6	84	55	72
5[d]	90	67	73
$CuCl_2$	29	13	58

[a] Reaction conditions: DMP (1 mmol), NaOH (1 mmol), H_2O_2 (20 μL), and catalyst (0.01 mmol) in 3 mL of water for 8 h at 50 °C. [b] Conversions and isolated yields based on the DMP; average of two runs. [c] Selectivity = 100[PPE]/([PPE] + [DPQ]). [d] Second reuse.

complexes have an obvious comparative advantage in the oxidative coupling of DMP.

In addition, the coordination environments of metal centers also influence the catalytic activities. In general, a lower coordination number leads to a higher catalytic activity. And the coordinated water molecules in the complexes are easy leaving groups and can be readily replaced by the substrate; thus, it is easier for the phenolate anion to enter the metal coordination sphere when metal centers are coordinated by water molecules, further enhancing the catalytic activity. For example, complexes **1**−**3** with the same reactants but different coordination geometries exhibit different catalytic properties. Specifically, in **1**, there is only one type of six-coordinated Co(II) center. The results show that complex **1** affords a moderate catalytic effect, while the Co(II) centers in complex **2** have two different coordination environments. One is four-coordinated, and the other is six-coordinate with one coordinated water molecule. Complex **2** gives relatively high conversion and yield of PPE among the three complexes. The Co(II) centers in complex **3** also have two kinds of coordination modes, but both of them are six-coordinated with one or two coordinated water molecules. Complex **3** provides relatively high selectivity of PPE among the three complexes. On the other hand, the pore size also exerts a profound influence on the catalytic activities. The larger the pore is, the better the catalytic activity is. Concretely, large cavities in complexes could

dx.doi.org/10.1021/cg101494t |*Cryst. Growth Des.* 2011, 11, 2183–2193

accommodate more substrates binding to Cu(II) centers to facilitate this oxidative coupling, and thus, the higher yield of PPE is observed. This is also in agreement with the experimental result. For example, the pore volumes for **1**−**3** are 274.8, 554.1, and 81.9 Å^3 (**2** > **1** > **3**), respectively, which are calculated by PLATON. The yields of PPE also follow the order 32% for **1**, 44% for **2**, and 25% for **3**. We also found that complexes **3** and **4** provide similar results. This may be due to the fact that they are isostructural. Comparing the two copper complexes, it is found that the Cu(II) centers in complex **5** have higher coordination numbers than those of **6**, but complex **5** generally shows the highest activity within this system. This is possibly attributed to a little larger pore volume of **5** (pore volume for **5**, 53.0 Å^3; for **6**, 45.0 Å^3) and the nature of coordinated anions, which may favor the coordination of the substrate to Cu(II) centers to promote the oxidative coupling reaction. It is evident that the metal centers, coordinated anions, pore sizes, and coordination geometries of the structures have great influence on the catalytic activities. As a result, further structure modification for MOFs could be realized through objective molecular design and synthesis, and then enhance the catalytic properties for desired applications.

Taking into account that complex **5** was high catalytically active in the green catalysis process of the oxidative coupling of DMP, we take the complex as an example to study the stability after catalytic reaction. After completion of the polymerization, simple filtration of the reaction mixture allowed the separation of the solid-state catalyst from the product-containing solution. After washing with $CHCl_3$ several times, the catalyst was characterized by powder XRD. The XRD patterns of the catalyst before and after catalytic reaction are the same, which indicates that the structural integrity of complex **5** was maintained during the catalytic process (Figure S3 of the Supporting Information). Then the complex was reused for the next cycle. The result showed that complex **5** could be used for the next cycle without significant loss of selectivity and only a slight loss of conversion was observed. The slight loss of conversion may be caused by the loss of the catalyst during the recovery process. The complex exhibits a great potential as recyclable catalyst.

CONCLUSIONS

In summary, we have synthesized and characterized six new MOFs based on aromatic polycarboxylate and a long flexible bis(triazole) ligand, which show rich structural features. The results of this study illustrate that the coordination modes of carboxylate ligand and the nature of the neutral ligands play important roles in the construction of MOFs. The catalytic activities of the complexes indicate that the copper complexes may be good catalysts for the oxidative coupling of 2,6-dimethylphenol (DMP). It is anticipated that more metal complexes containing neutral ligands and aromatic carboxylate anions with interesting structures as well as physical properties will be synthesized.

ASSOCIATED CONTENT

Supporting Information. X-ray crystallographic files in CIF format and powder X-ray patterns for **1**−**6**. This material is available free of charge via the Internet at http://pubs.acs.org.

AUTHOR INFORMATION

Corresponding Author

*Fax: (86) 0371-67761744. E-mail: houhongw@zzu.edu.cn.

ACKNOWLEDGMENT

This work was financially supported by the National Natural Science Foundation (Nos. 20971110 and 91022013), Program for New Century Excellent Talents of Ministry of Education of China (NCET-07-0765), the Outstanding Talented Persons Foundation of Henan Province, and The Ministry of Science and Technology of China for the International Science Linkages Program (2009DFA50620).

REFERENCES

(1) (a) Han, S. S.; Goddard, W. A., III. *J. Am. Soc. Chem.* **2007**, *129*, 8422. (b) Kaczorowski, T.; Justyniak, I.; Lipinska, T.; Lipkowski, J.; Lewinski, J. *J. Am. Chem. Soc.* **2009**, *131*, 5393. (c) Eddaoudi, M.; Moler, D. B.; Li, H.; Chen, B.; Reineke, T. M.; O'Keeffe, M.; Yaghi, O. M. *Acc. Chem. Res.* **2001**, *34*, 319. (d) Fang, Q. R.; Zhu, G. S.; Xue, M.; Sun, J. Y.; Wei, Y.; Qiu, S. L.; Xu, R. R. *Angew. Chem., Int. Ed.* **2005**, *44*, 3845. (e) Yamauchi, Y.; Yoshizawa, M.; Fujita, M. *J. Am. Chem. Soc.* **2008**, *130*, 5832. (f) Xu, J.; Pan, Z. R.; Wang, T. W.; Li, Y. Z.; Guo, Z. J.; Batten, S. R.; Zheng, H. G. *CrystEngComm* **2010**, *12*, 612. (g) Zhang, F. W.; Li, Z. F.; Ge, T. Z.; Yao, H. C.; Li, G.; Lu, H. J.; Zhu, Y. Y. *Inorg. Chem.* **2010**, *49*, 3776.

(2) (a) Yoshizawa, M.; Nagao, M.; Umemoto, K.; Biradha, K.; Fujita, M.; Sakamoto, S.; Yamaguchi, K. *Chem. Commun.* **2003**, 1808. (b) Chen, B.; Fronczek, F. R.; Maverick, A. W. *Chem. Commun.* **2003**, 2166. (c) Batten, S. R.; Murray, K. S. *Coord. Chem. Rev.* **2003**, *246*, 103. (d) Chen, B.; Ma, S.; Zapata, F.; Fronczek, F. R.; Lobkovsky, E. B.; Zhou, H. C. *Inorg. Chem.* **2007**, *46*, 1233. (e) Chen, S. M.; Lu, C. Z.; Zhang, Q. Z.; Liu, J. H.; Wu, X. Y. *Eur. J. Inorg. Chem.* **2005**, 423. (f) Cho, S. H.; Ma, B.; Nguyen, S. T.; Hupp, J. T.; Albrecht-Schmitt, T. E. *Chem. Commun.* **2006**, 2563.

(3) (a) Ye, B. H.; Ding, B. B.; Weng, Y. Q.; Chen, X. M. *Cryst. Growth Des.* **2005**, *5*, 801. (b) Qi, Y.; Che, Y. X.; Zheng, J. M. *Cryst. Growth Des.* **2008**, *8*, 3602. (c) Zhu, S. R.; Zhang, H.; Zhao, Y. M.; Shao, M.; Wang, Z. X.; Li, M. X. *J. Mol. Struct.* **2008**, *892*, 420. (d) Su, Z.; Xu, J.; Fan, J.; Liu, D. J.; Chu, Q.; Chen, M. S.; Chen, S. S.; Liu, G. X.; Wang, X. F.; Sun, W. Y. *Cryst. Growth Des.* **2009**, *9*, 2801. (e) Du, M.; Jiang, X. J.; Zhao, X. J. *Inorg. Chem.* **2007**, *46*, 3984.

(4) (a) Mu, Y. J.; Song, Y. J.; Wang, C.; Hou, H. W.; Fan, Y. T. *Inorg. Chim. Acta* **2010**, *365*, 167. (b) Hu, J. Y.; Li, J. P.; Zhao, J. A.; Hou, H. W.; Fan, Y. T. *Inorg. Chim. Acta* **2009**, *362*, 5023. (c) Meng, X. R.; Song, Y. L.; Hou, H. W.; Han, H. Y.; Xiao, B.; Fan, Y. T.; Zhu, Y. *Inorg. Chem.* **2004**, *43*, 3528. (d) Ren, C.; Liu, P.; Wang, Y. Y.; Huang, W. H.; Shi, Q. Z. *Eur. J. Inorg. Chem.* **2010**, 5545. (e) Ren, C.; Hou, L.; Liu, B.; Yang, G. P.; Wang, Y. Y.; Shi, Q. Z. *Dalton Trans.* **2011**, *40*, 793.

(5) (a) Yang, E. C.; Liu, Z. Y.; Shi, X. J.; Liang, Q. Q.; Zhao, X. J. *Inorg. Chem.* **2010**, *49*, 7969. (b) Wang, X. L.; Bi, Y. F.; Lin, H. Y.; Liu, G. C. *Cryst. Growth Des.* **2007**, *7*, 1086.

(6) Sheldrick, G. M. *Acta Crystallogr.* **2008**, *A64*, 112.

(7) Zhang, E. P.; Hou, H. W.; Han, H. Y.; Fan, Y. T. *J. Organomet. Chem.* **2008**, *693*, 1927.

(8) (a) Qi, Y.; Luo, F.; Che, Y. X.; Zheng, J. M. *Cryst. Growth Des.* **2008**, *8*, 606. (b) Bai, H. Y.; Ma, J. F.; Yang, J.; Zhang, L. P.; Ma, J. C.; Liu, Y. Y. *Cryst. Growth Des.* **2010**, *10*, 1946. (c) Yang, W. B.; Lin, X.; Blake, A. J.; Wilson, C.; Hubberstey, P.; Champness, N. R.; Schröder, M. *Inorg. Chem.* **2009**, *48*, 11067. (d) Wang, L.; Gu, W.; Deng, J. X.; Liu, M. L.; Xu, N.; Liu, X. *Z. Anorg. Allg. Chem.* **2009**, *636*, 1124.

(9) (a) Li, C. Y.; Liu, C. S.; Li, J. R.; Bu, X. H. *Cryst. Growth Des.* **2007**, *7*, 286. (b) Gao, E. Q.; Xu, Y. X.; Yan, C. H. *CrystEngComm* **2004**, *6*, 298.

(10) (a) Sun, H. L.; Gao, S.; Ma, B. Q.; Batten, S. R. *CrystEngComm* **2004**, *6*, 579. (b) Martin, D. P.; Supkowski, R. M.; LaDuca, R. L. *Cryst.*

Growth Des. **2008**, *8*, 3518. (c) Ma, L. F.; Wang, L. Y.; Wang, Y. Y.; Batten, S. R.; Wang, J. G. *Inorg. Chem.* **2009**, *48*, 915.

(11) (a) Chen, S. S.; Fan, J.; Okamura, T.; Chen, M. S.; Su, Z.; Sun, W. Y.; Ueyama, N. *Cryst. Growth Des.* **2010**, *10*, 812. (b) Yang, G. S.; Lan, Y. Q.; Zang, H. Y.; Shao, K. Z.; Wang, X. L.; Su, Z. M.; Jiang, C. J. *CrystEngComm* **2009**, *11*, 274. (c) Blatov, V. A.; Carlucci, L.; Ciani, G.; Proserpio, D. M. *CrystEngComm* **2004**, *6*, 377.

(12) (a) Fan, J.; Yee, G. T.; Wang, G. B.; Hanson, B. E. *Inorg. Chem.* **2006**, *45*, 599. (b) Tan, H. Y.; Zhang, H. X.; Ou, H. D.; Dang, B. S. *Inorg. Chim. Acta* **2004**, *357*, 869.

(13) (a) Liu, Y. Y.; Ma, J. F.; Yang, J.; Su, Z. M. *Inorg. Chem.* **2007**, *46*, 3027. (b) Liu, F. C.; Zeng, Y. F.; Jiao, J.; Bu, X. H.; Ribas, J.; Batten, S. R. *Inorg. Chem.* **2006**, *45*, 2776. (c) Yu, Q.; Li, C. P.; Zhang, Z. H.; Du, M. *Polyhedron* **2009**, *28*, 2347.

(14) (a) Addison, A. W.; Rao, T. N.; Reedijk, J.; Rijn, J. V.; Verschoor, G. C. *J. Chem. Soc., Dalton Trans.* **1984**, 1349. (b) Burchell, T. J.; Eisler, D. J.; Puddephatt, R. J. *Inorg. Chem.* **2004**, *43*, 5550.

(15) Yang, E. C.; Feng, W.; Wang, J. Y.; Zhao, X. J. *Inorg. Chim. Acta* **2010**, *363*, 308.

(16) Wen, L. L.; Wang, F.; Feng, J.; Lv, K. L.; Wang, C. G.; Li, D. F. *Cryst. Growth Des.* **2009**, *9*, 3581.

(17) Yan, Y.; Wu, C. D.; He, X.; Sun, Y. Q.; Lu, C. Z. *Cryst. Growth Des.* **2005**, *5*, 821.

(18) (a) Fujita, M.; Kwon, Y. J.; Washizy, S.; Ogura, K. *J. Am. Chem. Soc.* **1994**, *116*, 1151. (b) Tannenbaum, R. *Chem. Mater.* **1994**, *6*, 550. (c) Seo, J. S.; Whang, D.; Lee, H.; Jun, S. I.; Oh, J.; Jeon, Y. J.; Kim, K. *Nature* **2000**, *404*, 982. (d) Kondo, M.; Shimamura, M.; Noro, S.; Minakoshi, S.; Asami, A.; Seki, K.; Kitagawa, S. *Chem. Mater.* **2000**, *12*, 1288. (e) Fujita, M.; Umemota, K.; Yoshizawa, M.; Fujita, N.; Kusukawa, T.; Biradha, K. *Chem. Commun.* **2001**, 509. (f) Han, H. Y.; Zhang, S. J.; Hou, H. W.; Fan, Y. T.; Zhu, Y. *Eur. J. Inorg. Chem.* **2006**, 1594. (g) Xiao, B.; Hou, H. W.; Fan, Y. T. *J. Organomet. Chem.* **2007**, *692*, 2014.

(19) (a) Liu, Y.; Pang, Q. H.; Meng, X. G.; Liu, F. R.; Li, J. M.; Du, J.; Hu, C. W. *J. Appl. Polym. Sci.* **2010**, *118*, 2043. (b) Sadeghi, F.; Tremblay, A. Y.; Kruczek, B. J. *Appl. Polym. Sci.* **2008**, *109*, 1454. (c) Li, X. H.; Meng, X. G.; Pang, Q. H.; Liu, S. D.; Li, J. M.; Du, J.; Hu, C. W. *J. Mol. Catal. A: Chem.* **2010**, *328*, 88. (d) Sakar, D.; Cankurtaran, O.; Karaman, F. *Plast., Rubber Compos.* **2008**, *37*, 276.

(20) (a) Boldron, C.; AromÍ, G.; Challa, G.; Gamez, P.; Reedijk, J. *Chem. Commun.* **2005**, 5808. (b) Saito, K.; Tago, T.; Masuyama, T.; Nishide, H. *Angew. Chem., Int. Ed.* **2004**, *43*, 730. (c) Baesjou, P. J.; Driessen, W . L.; Challa, G.; Reedijk, J. *J. Am. Chem. Soc.* **1997**, *119*, 12590. (d) Gao, J.; Reibenspies, J. H.; Martell, A. E. *Inorg. Chim. Acta* **2002**, *338*, 157.

(21) Maurya, M. R.; Jain, I.; Titinchi, S. J. J. *Appl. Catal. A: Gen.* **2003**, *249*, 139.

(22) Guieu, S. J .A.; Lanfredi, A. M. M.; Massera, C.; Pachón, L. D.; Gamez, P.; Reedijk, J. *Catal. Today* **2004**, *96*, 259.